Progress In Electromagnetics Research C, Vol. 78, 19–31, 2017

Compact Antennas with Reduced Self Interference for Simultaneous Transmit and Receive

Gregory Makar[1, *], Daniel Kim[1], Nghi Tran[2], and Tutku Karacolak[1]

Abstract—A microstrip antenna system operating in the 2.4 GHz WLAN band is presented for in-band full-duplex operation. The design includes a patch antenna fed by a 180° hybrid. Two feeding methods are presented, probe and aperture. The measured bandwidths are 2.5% (60 MHz) and 2.1% (50 MHz) for the probe fed and aperture fed, respectively. The probe fed system reaches measured isolation (S_{21}) < -50 dB and the aperture fed < -45 dB in a reflective environment. The design also has low cross polarization, reasonable gain values, and a very low envelope correlation coefficient (< 0.01).

1. INTRODUCTION

Modern wireless communication devices are becoming more populous, crowding the frequency spectrums assigned for their use. Current systems operate in half-duplex mode in order to avoid the high levels of self-interference that occur between the receiving and transmitting elements (see Fig. 1). Avoiding the issue of the transmitting signal interfering with the receiving signal requires operation at either different times or at different frequencies. However, prospects for creating an in-band full-duplex system, which would allow for transmitting and receiving on the same frequency at the same time, have shown that full-duplex is feasible [1–6]. Ideally, this would allow twice as many devices to make use of a given spectrum at any time.

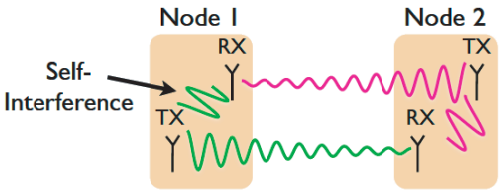

Figure 1. Self-interference in a full-duplex system.

Multiple approaches prior to the analog to digital (ADC) converter stage have been proposed in physical design in order to reduce self-interference. These cancellation methods include antenna separation, polarization diversity, using directional antennas, and placing absorptive shielding [7–9]. Although increasing the spacing and placing absorbers between antenna elements will provide high isolation, these techniques are not appropriate for compact size devices. Multiple antennas (two or more)have also been used to further improve the self-interference suppression. In [10], two transmitting antennas are located asymmetrically around a single receive antenna (d and $d + \lambda/2$) so that transmit

Received 12 May 2017, Accepted 28 August 2017, Scheduled 14 September 2017
* Corresponding author: Tutku Karacolak (tutku.karacolak@wsu.edu).
[1] School of Engineering and Computer Science, Washington State University Vancouver, Washington, USA. [2] Department of Electrical and Computer Engineering, University of Akron, Ohio, USA.

signals add destructively at the receiver due to an 180° phase difference. This method achieves about 40 dB of isolation, however it brings several limitations: (i) the receive antenna should receive the 180° out of phase signal only at the center frequency, (ii) the configuration of using multiple antennas is not feasible for handheld devices where space is limited,and (iii) use of multiple antennas creates nulls in the far field and degrades radiation pattern. To overcome the above shortcomings, a single antenna is used to transmit and receive simultaneously by incorporating a circulator combined with analog cancellation tools based on a balun, variable attenuators, and delay lines [11, 12]. A circulator can achieve approximately 20 dB of added isolation in this manner, with the loss of an increase in device cost and size. In [9], using commercially available hardware, a self-interference suppression level of 46 dB is experimentally demonstrated in a highly reflective indoor environment implementing a combination of directional isolation, absorptive shielding, and cross-polarization. However, the antenna separation is not less than 35 cm, thus rendering the device too large to be useful in many applications.

For a compact and power-efficient architecture, the 180° ring hybrid structure is considered in a recent work [13]. The design includes two closely spaced monopoles excited by the 180° hybrid. The proposed architecture achieves 40 dB isolation in a reflective environment within a compact physical size ($85 \times 62 \times 1.5\,\text{mm}^3$). In a design utilizing the 180° hybrid, the difference input port of the hybrid is used as the transmit port while the sum input port is connected to the receive port. As seen in Fig. 2, the remaining ports (2 and 4) can then be connected to identical and symmetrically placed antennas. The input at port 1 is excited, creating equal but out-of-phase components at ports 2 and 4 that combine in the far field but cancel in the near field. Likewise, the reflected powers at ports 2 and 4 are equal and out-of-phase, so they destroy each other at port 3, but any received signal that is input to ports 2 and 4 is summed at port 3. Alternatively, rather than use two separate, identical antennas, a single antenna can be used as long as ports 2 and 4 are connected to it in the same manner for differential feeding.

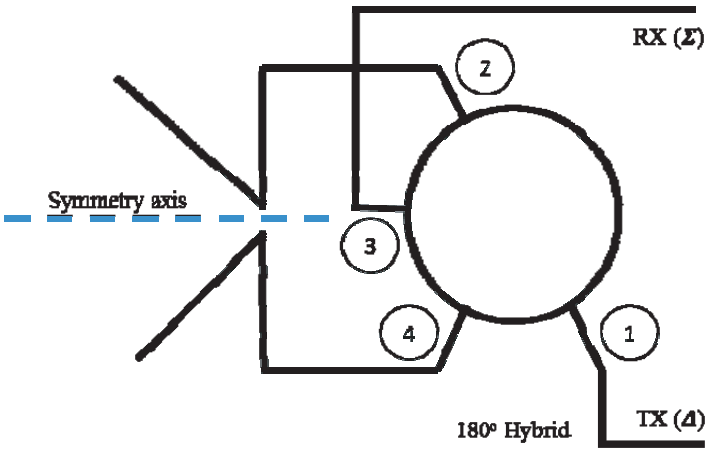

Figure 2. Full-duplex node architecture utilizing 180° hybrid.

In this study, we present two designs using a radiating patch antenna excited by ports 2 and 4 of a ring hybrid structure to accomplish in-band full-duplex operation. Both designs feature high isolation and low cross polarization. These designs differ in the method of feeding the patch from the hybrid, one using a probe feed, the other an aperture feed. The design will separate the patch and ring hybrid structure by two substrates with a ground plane between them. The probe fed design will require two conductors to go through both substrates without being in electrical contact with the ground plane. The aperture fed design will require only that some of the copper ground plane be removed, with no interior cutting of the substrate necessary. The designs will be discussed, especially focusing on differences in construction required when switching the feed style. Then, the simulated and measured results of the designs will be presented on their own and in comparison, and their possible impact on in-band full-duplex systems will be discussed.

2. ANTENNA DESIGN

The two devices are both designed to operate in the 2.4 GHz band, which heavily affects the dimensions for the patch antenna as well as the ring hybrid structure. The patch is printed on the top side of the first substrate, and the ring hybrid feeding network is designed on the bottom side of the lower substrate. This structure has the advantage of blocking radiation from feedlines. Parametric optimization was used while simulating each design in ANSYS HFSS to achieve operation at the desired frequency. Both designs use two FR4 epoxy substrates of relative permittivity 4.1, fastened using 3M super 77 Multipurpose Adhesive.

2.1. Probe Fed Design

The first design excites a square patch differentially using two out of phase probes to avoid undesired leakage radiation and thereby decrease the level of cross polarization. The probe fed antenna places the patch on a 1.5 mm substrate and the ring hybrid on a 0.7 mm substrate, both opposite their respective fastened side. The patch is 30.5 mm along each side, while the hybrid is 17.2 mm at its inner radius. Top and bottom views of the antenna are given in Fig. 3, and full dimensions for the design are given in Table 1. The patch is rotated such that were a line to connect the feed holes, it would not be parallel to one side of the patch. Instead, it is perpendicular to a corner of the patch, as this symmetry provides better isolation characteristics. The probes used for feeding are connected to the patch and to arms 2 and 4 of the ring hybrid. Arm 1 of the ring hybrid provides the transmitted signal, while arm 3 is used for the received signal. Also note that arms 2 and 4 become less wide as they near the ring hybrid. This improves matching of the ring hybrid to the assumed 50 Ω connection.

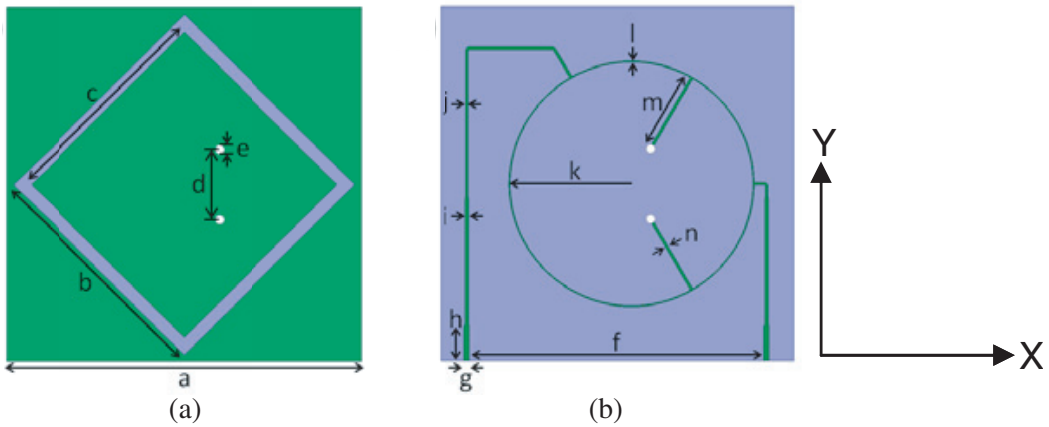

Figure 3. (a) Top and (b) bottom layers of probe fed antenna.

Table 1. Dimensions of probe fed antenna (in mm).

$a = 50$	$b = 34$	$c = 30.5$	$d = 9.9$	$e = 1.265$
$f = 41.65$	$g = 0.73$	$h = 5$	$i = 0.537$	$j = 0.38$
$k = 17.2$	$l = 0.15$	$m = 11.48$	$n = 0.38$	

2.2. Aperture Fed Design

The second design uses two rectangular slots on the ground plane to couple energy from the transmit port (arm 1 of the ring hybrid) to the patch. However, rather than use the isolation port (arm 3) of the ring hybrid for the received signal, the receive port is directly connected to the patch antenna through a microstrip line. This adaptation generates orthogonal linear polarizations in the same radiating

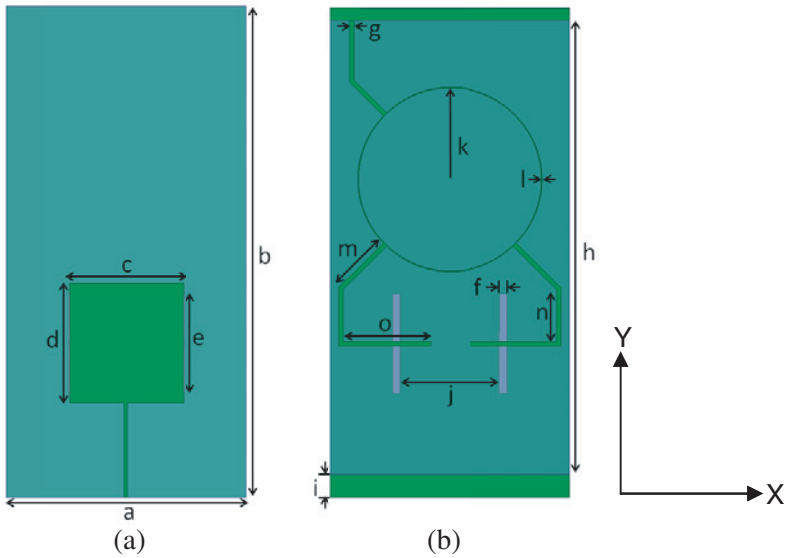

(a) (b)

Figure 4. (a) Top and (b) bottom layers of aperture fed antenna.

Table 2. Dimensions of aperture fed antenna (in mm).

$a = 60$	$b = 123$	$c = 28.3$	$d = 30$	$e = 25$
$f = 1.81$	$g = 1.15$	$h = 114$	$i = 6$	$j = 25.21$
$k = 23$	$l = 0.18$	$m = 15.73$	$n = 13.17$	$o = 23$

structure. Transmitter and receiver ports excite linear polarizations in the horizontal and vertical planes, respectively, to achieve high isolation and low cross polarization. Top and bottom views of the antenna are given in Fig. 4, and full dimensions for the design are given in Table 2. As seen, the aperture fed antenna uses two 1.5 mm substrates, while again separating the patch and hybrid, placing them opposite one another by being opposite their fastened side. The patch is 30 mm by 28.3 mm, the latter placing it above the aperture slots, which are placed 25.21 mm apart. The ring hybrid is 23 mm at its inner radius.

The sides of the patch run parallel and perpendicular, respectively, to the length of the apertures that are cut out of the ground plane. Arms 2 and 4 of the ring hybrid provide the differential feeding for the patch, and arm 1 provides the transmitted signal. Note that the isolated port of the ring hybrid is removed. We have seen that the modified version still achieves good matching characteristics at the transmitter port and equally splits power into two out of phase components. The radiation patterns without the isolated port are not significantly affected. Avoiding the termination of a matched load (50 Ω) also simplifies the fabrication process.

3. EXPERIMENTAL RESULTS

The results are presented individually for the designs, followed by a comparison of the designs' results.

3.1. Probe Fed Design

The designs are fabricated with an LPKF S-63milling machine. The transmit and receive ports of both antennas use 50 ohm SMA connectors for measurement purposes. The probes used for feeding their respective design are copper wires soldered to the patch and to arms 2 and 4 of the ring hybrid. Using the same material for the probes as the patch and ring hybrid eliminates material inconsistencies that might affect the final results, though solder cannot be avoided. The substrate with the printed hybrid is $50 \times 50 \times 0.7\,\text{mm}^3$, while the substrate with the printed patch is $34 \times 34 \times 1.5\,\text{mm}^3$ in size. The patch

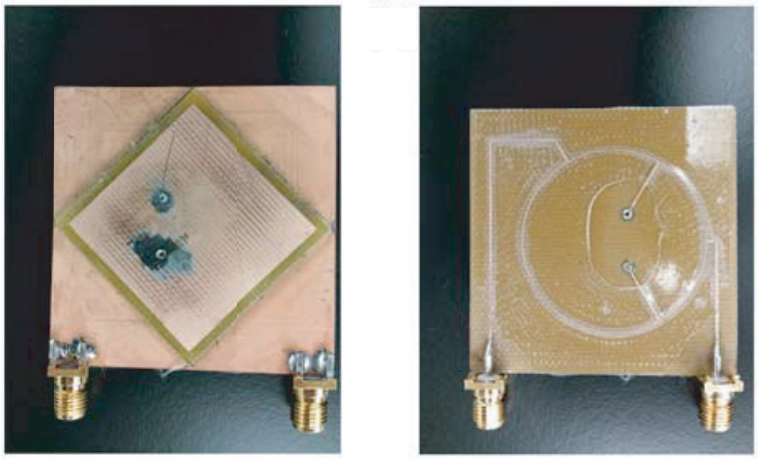

(a) (b)

Figure 5. (a) Top and (b) bottom of fabricated probe fed antenna.

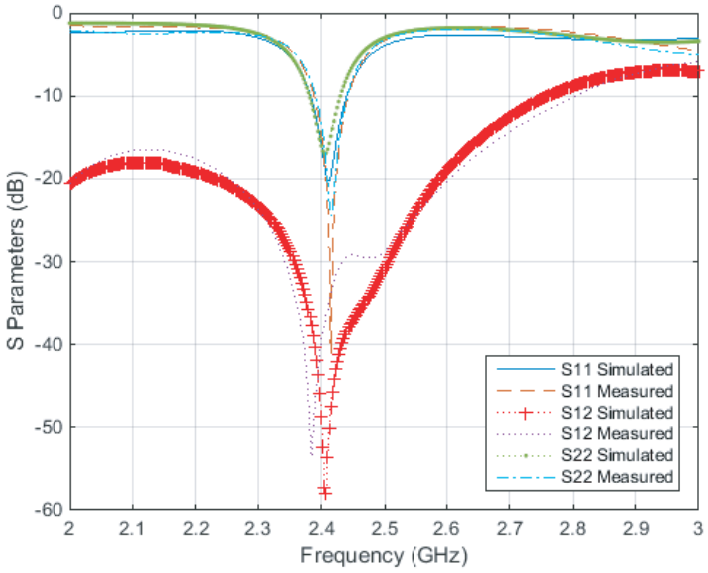

Figure 6. Simulated and measured S-parameters for the probe fed antenna.

substrate fits completely on the hybrid substrate, so the combined dimensions are $50 \times 50 \times 2.2\,\text{mm}^3$. The fabricated antenna can be seen in Fig. 5.

The probe fed antenna achieves a bandwidth of approximately 60 MHz, or 2.5% of 2.4 GHz, beginning at approximately 2.39 GHz. Both the transmit and receive ports achieve greater than 20 dB of return loss. The isolation peaks at greater than 50 dB, however there is a shift in the fabricated isolation from the simulated to approximately 2.38 GHz, just outside of the operational bandwidth. These results are shown in Fig. 6. This small shift from the simulated expectation could possibly be attributed to change in medium as the signal travels from copper trace through solder to copper pins, or a slight change in permittivity or thickness between the substrates due to the fastening substance. Fig. 7 shows surface current density at 2.4 GHz. When the transmit port is excited, high isolation is clearly observed between the two ports. The antenna has a directive radiation pattern in the z direction. This is demonstrated by the simulated co-polarized and cross-polarized radiation fields shown in Fig. 8, developed at 2.4 GHz for the x-z ($\phi = 0°$) and y-z ($\phi = 90°$) planes. As seen, the cross-polarization values are 25 to 40 dB lower than the co-polarization values, and the antenna provides a broad coverage

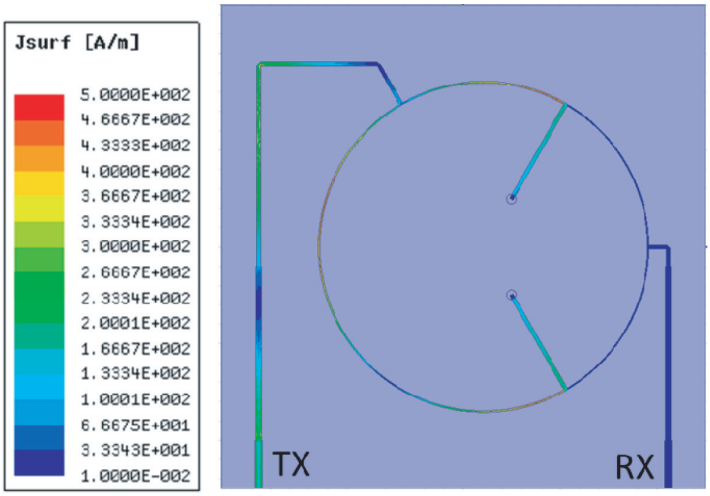

Figure 7. Surface current density for the probe fed antenna.

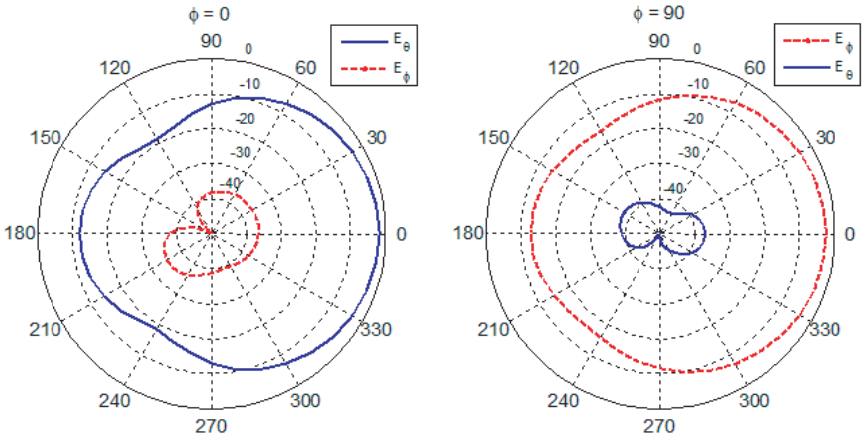

Figure 8. Simulated radiation patterns for (a) $\varphi = 0°$ and (b) $\varphi = 90°$ for the probe fed antenna.

area with a half power beamwidth (HPBW) around 60°. The gain of this antenna is greater than 6 dB at its peak value at 2.4 GHz, seen in Fig. 9. The antenna also has a high efficiency at 2.4 GHz, reaching nearly 90% shown in Fig. 10. Using the radiating efficiency and S-parameters of the design the envelope correlation coefficient can be calculated using Equation (1), which follows:

$$|\rho_{ij}|^2 = \left| \frac{\left| S_{ii}^* S_{ij} + S_{ji}^* S_{jj} \right|^2}{\left| \left(1 - |S_{ii}|^2 - |S_{ji}|^2\right) \left(1 - |S_{jj}|^2 - |S_{ij}|^2\right) \eta_i \eta_j \right|} \right| \tag{1}$$

Using this equation requires the assumption that the antenna system is itself lossless and that all incident waves are distributed uniformly in the surrounding environment [14]. The envelope correlation coefficient is an extremely useful calculation for expressing the effectiveness of an antenna in a MIMO system. As a STAR (simultaneous transmit and receive) system has the same ultimate goal of separating the transmit and receive signals in a compact antenna, this coefficient can be applied with merit to STAR systems as well. The envelope correlation coefficient for this design is below 0.1 for the entire 2 to 3 GHz sweep, with the value in the operating bandwidth being well below even 0.01, and is also displayed in Fig. 10. It is generally considered desirable to obtain a coefficient below 0.3, and this antenna has a coefficient much less than that.

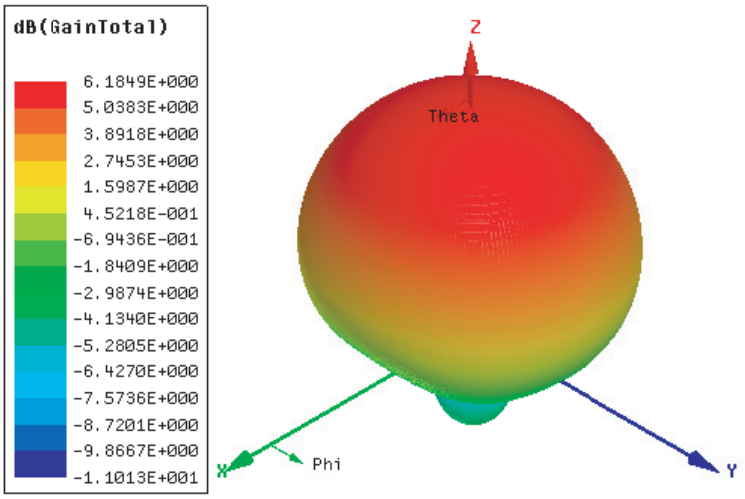

Figure 9. Gain pattern at 2.4 GHz for probe fed antenna.

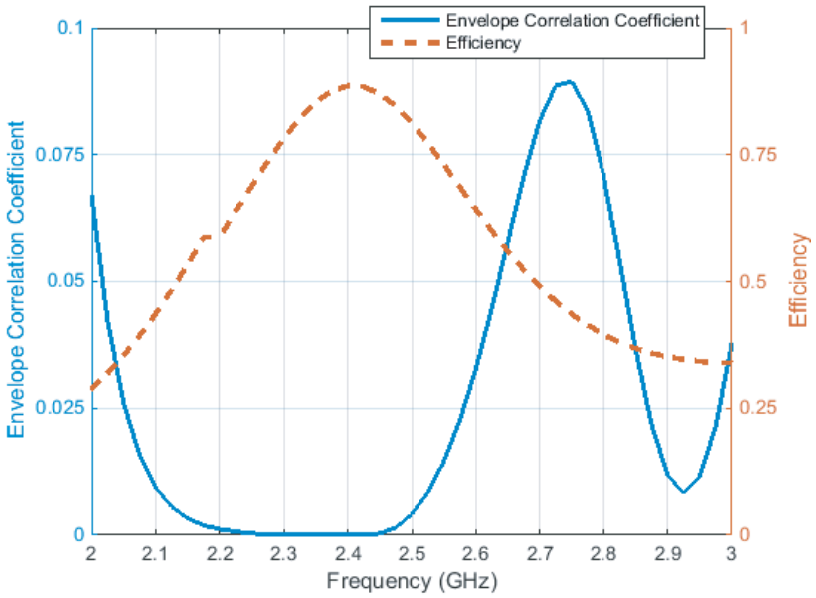

Figure 10. Efficiency and ECC of probe fed antenna.

3.2. Aperture Fed Design

The apertures used for feeding their respective design are cut from the copper ground plane between the two substrates. This design requires a much larger fabrication than the probe fed design, primarily due to patch's placement with regards to the ring hybrid. Instead of being placed directly above the ring hybrid, the patch must be placed between the apertures which are placed with relation to the feeding arms. Due to this, the substrate with the printed hybrid is $114 \times 60 \times 1.5\,\text{mm}^3$, while the substrate with the printed patch is $123 \times 60 \times 1.5\,\text{mm}^3$, though the combined dimensions are $123 \times 60 \times 3\,\text{mm}^3$. The 9 mm difference in the largest dimension of the design allows for the SMA connectors to be easily soldered. The fabricated antenna is displayed in Fig. 11.

The aperture fed antenna proved more difficult to fabricate, and the resulting antenna has greater shifts from the simulated values. The bandwidth of the antenna is approximately 50 MHz, or 2.1%, and has been shifted to center at 2.36 GHz. At this range the isolation falls between 40 and 45 dB, and has a

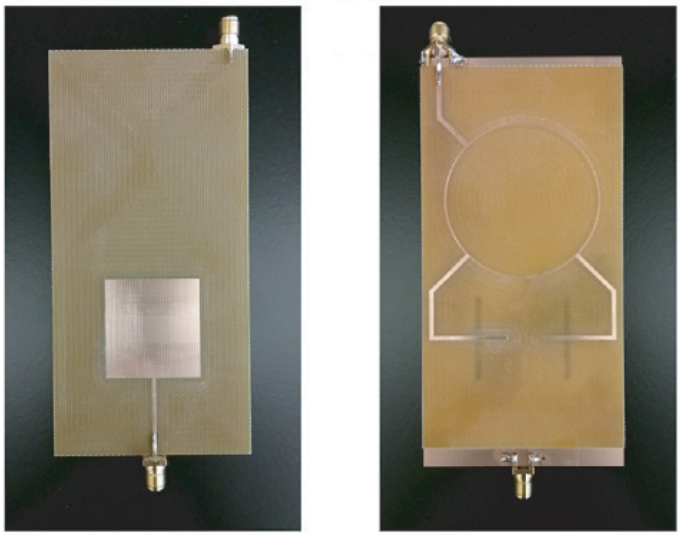

(a) (b)

Figure 11. (a) Top and (b) bottom of fabricated aperture fed antenna.

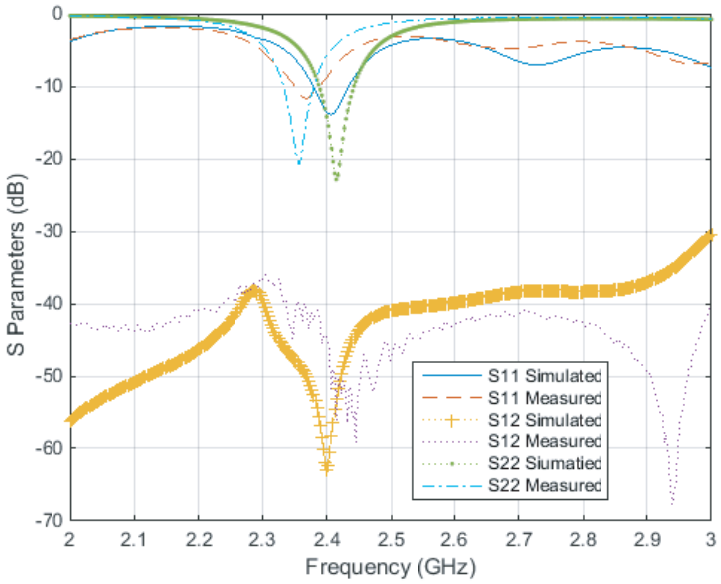

Figure 12. Simulated and measured S-parameters for the aperture fed antenna.

maximum near 60 dB, however the isolation is never less than 40 dB in the 2 to 3 GHz swept frequency range, as shown in Fig. 12. This is due to the orthogonal polarization of the receiver and transmitter signals. Despite the consistently large amount of isolation, there is a dip at the simulated and fabricated operational frequency bands due to the ring hybrid, which for this design offers more than 20 dB of greater isolation at the desired frequency. Unfortunately, the fabricated design's dip does not occur at the frequency of operation, but nearer to the simulated values. Many possible explanations for the shift in frequency, and the degradation in the return loss of the transmitter, are being followed, including the fastening substance and errors caused due to lack of perfect assembly of the substrates.Surface current density of the antenna is shown in Fig. 13. As seen, receive port is isolated from transmit port.

Figures 14 and 15 show the co-polarized and cross-polarized radiation patterns of the antenna at 2.4 GHz for transmit and receive modes, respectively. It can be seen that when the receive port is excited,

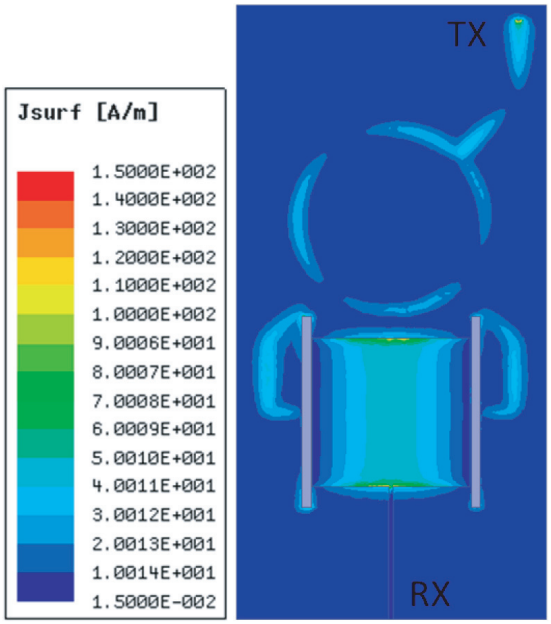

Figure 13. Surface current density for the aperture fed antenna.

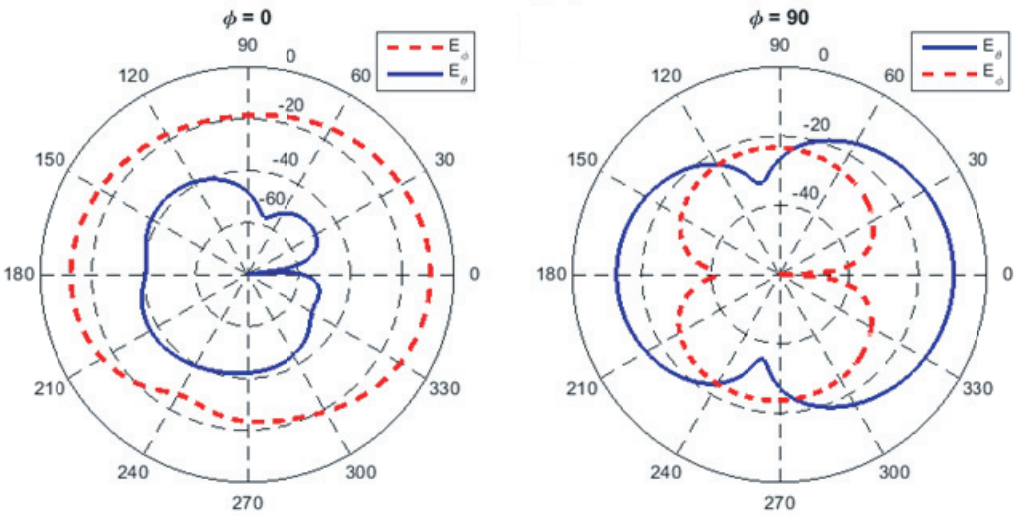

(a) (b)

Figure 14. Simulated radiation patterns for (a) $\varphi = 0°$ and (b) $\varphi = 90°$ for transmission of the aperture fed antenna.

the cross-polarization is lower than −20 dB within the range of observation angle ±90°. The transmit mode has higher cross-polarization values compared to receiving case. Although cross-polarization is greater than −15 dB at off-boresight observation angles, it is still better than −20 dB at boresight. The gain is high in both cases.When excited by the transmit port the peak gain at 2.4 GHz is greater than 6.4 dB, with a lobe of 3 dB in the opposite direction as well, seen in Fig. 16. For the receiving port, the peak gain is lower, just greater than 5 dB, as seen in Fig. 17. The efficiency of the antenna remains above 75% at all times. Using Equation (1) as stated above the simulated envelope correlation coefficient for this antenna can be calculated as well, and it is shown to never reach 0.01 between 2 and 3 GHz, and to be below 0.001 at the frequency band of interest. This low value is explained by both good efficiency and the extremely low isolation throughout. This value is again far below 0.3, suggesting effectiveness.

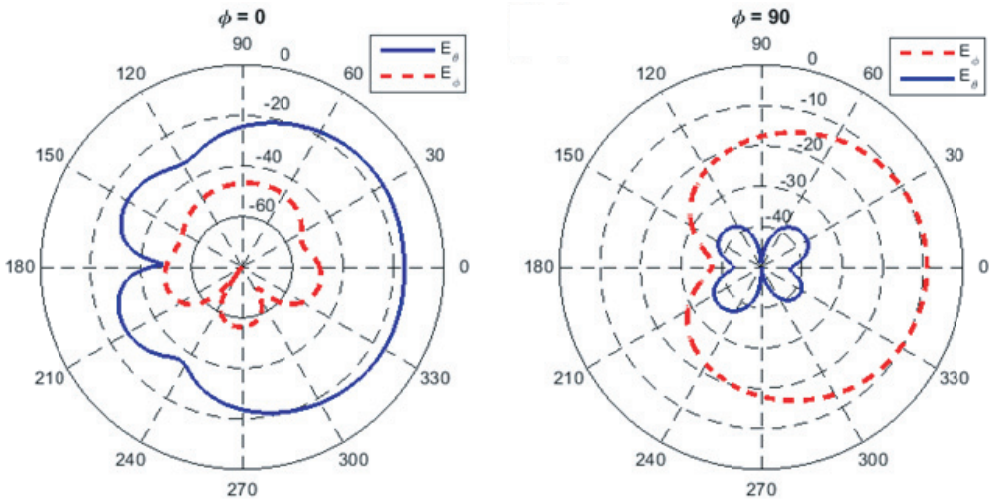

(a) (b)

Figure 15. Simulated radiation patterns for (a) $\varphi = 0°$ and (b) $\varphi = 90°$ for reception of the aperture fed antenna.

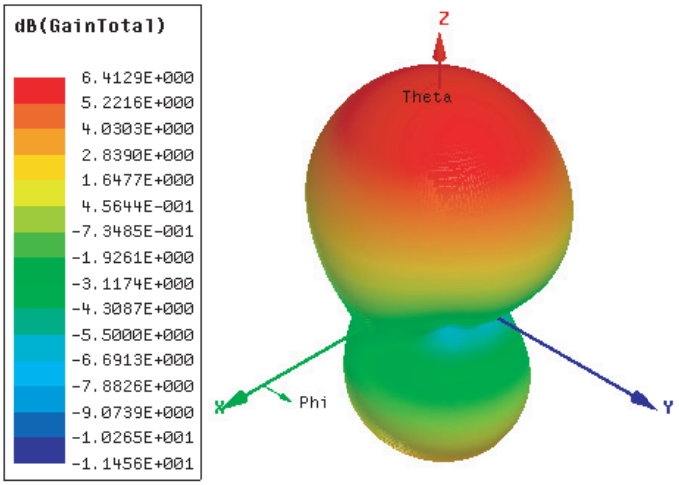

Figure 16. Gain pattern at 2.4 GHz for transmission of the aperture fed antenna.

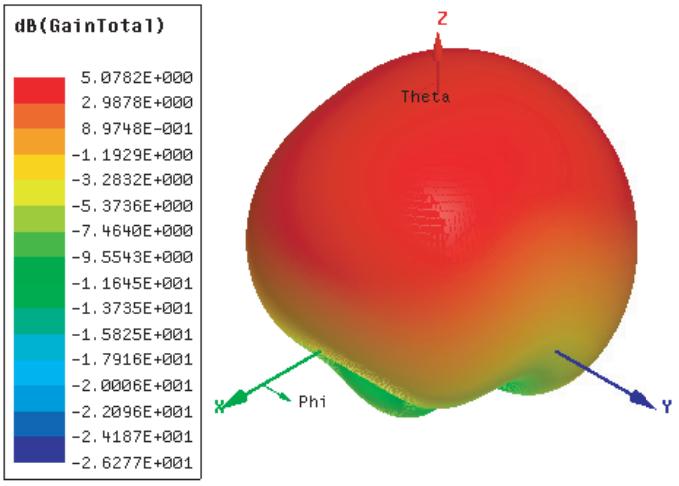

Figure 17. Gain pattern at 2.4 GHz for reception of the aperture fed antenna.

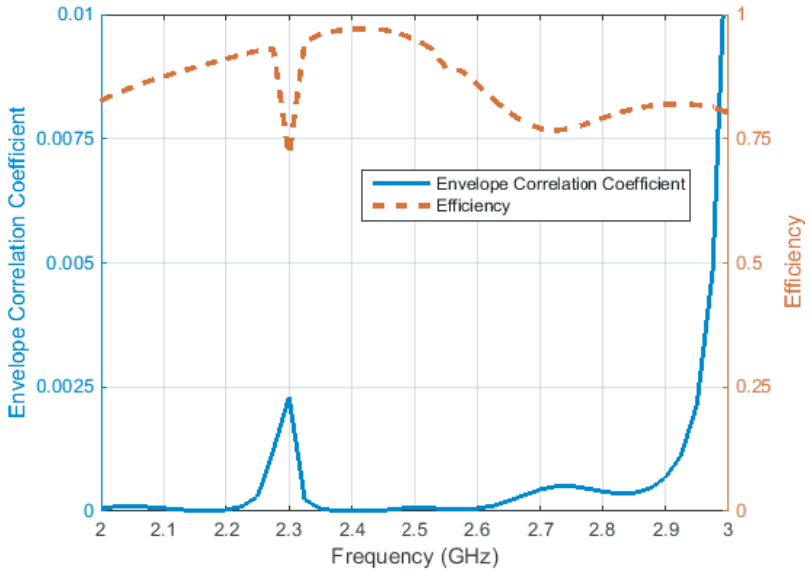

Figure 18. Efficiency and ECC of aperture fed antenna.

Both the efficiency and envelope correlation coefficient for this antenna are plotted in Fig. 18. These values use a case of an active transmit port for this antenna.

3.3. Comparison

Table 3 compares the performance of the proposed antennas (probe and aperture fed) with similar designs from the literature. As seen, both designs achieve high isolation (less than −40 dB) within reasonable bandwidths in a reflective environment. Proposed antennas also have compact size and can fit within most wireless devices. Compared to aperture fed antenna, the probe fed antenna has better impedance matching for both ports, as well as a reliable peak isolation value. However, the aperture fed antenna, if proper improvements can be made to the fabrication process, should offer greater bandwidth, especially for the isolation, than the probe fed can offer. The peak gain and efficiency for each design have high values at the desired frequency of operation, with the probe fed antenna peaking at this point while the aperture fed antenna has large values from 2 to 3 GHz. The peak values are comparable. The probe fed antenna has the advantage in terms of the radiation patterns achieving very low cross-

Table 3. Comparison of the proposed designs with literature.

	[15]	[16]	[17]	[9]	[13]	This Work Probe/Aperture
Minimum Isolation (dB)	−23 dB	−30 dB	−30 dB	−46 dB	−35 dB	−40 dB for both designs
Bandwidth (MHz)	55	200	115	25	130	60 / 50
Gain (dBi)	2.7	4.2	4	-	4	6/6.4
Size (mm^3)	22 × 59 × 0.8	100 × 50 × 0.8	125 × 100 × 0.8	Antenna separation > 350 mm	85 × 62 × 1.5	50 × 50 × 2.2 123 × 60 × 3

polarizations in both transmission and reception. However, the aperture design is still effective at accomplishing high levels of isolation with good radiation and high gain and efficiency, just as the probe fed is.

4. CONCLUSION

A patch antenna fed by a 180° ring hybrid is presented for in-band full-duplex applications. Two feeding methods are examined, probe fed and aperture fed. The self-interference between the transmit and receive ports has reached greatly reduced values in both cases. Isolation is shown to peak greater than 50 dB for the probe fed design and to be consistently greater than 40 dB in the band of interest for the aperture fed design. Fabrication proved especially difficult for the aperture fed patch and a focus on improving this would likely produce a superior result. A directive pattern with low cross polarization values is produced for both designs and each have an extremely low envelope correlation coefficient at the operating frequency band.

ACKNOWLEDGMENT

This work was supported by the National Science Foundation under Grant No. ECCS-1509052.

REFERENCES

1. Sabharwal, A., P. Schniter, D. Guo, D. Bliss, S. Rangarajan, and R. Wichman, "In-band full-duplex wireless: Challenges and opportunities," *IEEE J. Sel. Areas Commun.*, Vol. 32, No. 9, Sept. 2014.
2. Jain, M., J. I. Choi, T. Kim, D. Bharadia, S. Seth, K. Srinivasan, P. Levis, S. Katti, and P. Sinha, "Practical, real-time, full duplex wireless," *Proc. ACM Annu. Int. Conf. Mobile Computing Netw.*, 301–312, 2011.
3. Liu, G. F. R. Yu, H. Ji, V. C. M. Leung, and X. Li, "In-band full-duplex relaying: A survey, research issues and challenges," *IEEE Commun. Surveys and Tutorials*, Vol. 17, No. 2, 500–524, 2015.
4. Duarte, M. C. Dick, and A. Sabharwal, "Experiment-driven characterization of full-duplex wireless systems," *IEEE Trans. Wireless Commun.*, Vol. 11, 4296–4307, Dec. 2012.
5. Aryafar, E. M. A. Khojastepour, K. Sundaresan, S. Rangarajan, and M. Chiang, "MIDU: Enabling MIMO full duplex," *Proc. ACM Annu. Int. Conf. Mobile Computing Netw.*, 257–268, 2012.
6. Khojastepour, M. A., K. Sundaresan, S. Rangarajan, X. Zhang, and S. Barghi, "The case for antenna cancellation for scalable full-duplex wireless communications," *Proc. ACM Workshop Hot Topics Netw.*, 171–176, 2011.
7. Duarte, M. and A. Sabharwal, "Full-duplex wireless communications using off-the-shelf radios: Feasibility and first results," *Proc. Asilomar Conf. Signals, Syst., Comput.*, 1558–1562, Nov. 2010.
8. Everett, E., M. Duarte, C. Dick, and A. Sabharwal, "Empowering fullduplex wireless communication by exploiting directional diversity," *Proc. Asilomar Conf. Signals, Syst., Comput.*, 2002–2006, Nov. 2011.
9. Everett, E., A. Sahai, and A. Sabharwal, "Passive self-interference suppression for full-duplex infrastructure nodes," *IEEE Trans. on Wireless Comm.*, Vol. 13, No. 2, 680–694, 2013.
10. Choi, J. I., M. Jain, K. Srinivasan, P. Levis, and S. Katti, "Achieving single channel, full duplex wireless communication," *Proc. ACM Annu. Int. Conf. Mobile Computing Netw.*, 1–12, 2010.
11. Hong, S., J. Mehlman, and S. Katti, "Picasso: Flexible RF and spectrum slicing," *Proc. SIGCOMM*, 1–5, Aug. 2012.
12. Bharadia, D., E. McMilin, and S. Katti, "Full duplex radios," *ACM Sigcomm Computer Communication Review*, Vol. 43, No. 4, 375–386, Oct. 2013.
13. Makar, G., N. Tran, and T. Karacolak, "A high isolation monopole array with ring hybrid feeding structure for in-band full-duplex systems," *IEEE Antennas and Wireless Propagation Letters*, Vol. 16, 356–359, 2017.

14. Fernandez, S. C. and S. K. Sharma, "Multiband printed meandered loop antennas with MIMO implementations for wireless routers," *IEEE Antennas Wireless Propag. Lett.*, Vol. 12, 96–99, 2013.
15. Gong, Q., Y. Jiao, and S. Gong, "Compact MIMO antennas using a ring hybrid for WLAN applications," *Journal of Electromagnetic Waves and Applications*, Vol. 25, 431–441, 2011.
16. Wu, T., S. Fang, and K. Wong, "Printed diversity monopole antenna for WLAN operation," *Electronics Lett.*, Vol. 38, No. 25, 1625–1626, Dec. 2002.
17. Yang, C., Y. Yao, J. Yu, and X. Chen, "Novel compact multiband MIMO antenna for mobile terminal," *Int. J. of Antennas and Propag.*, Vol. 2012, Article ID 691681, 9 pages, 2012.